Journal of Magnetism and Magnetic Materials 398 (2016) 141–147

Contents lists available at ScienceDirect

Journal of Magnetism and Magnetic Materials

journal homepage: www.elsevier.com/locate/jmmm

Magnetic order of Y_3NiSi_3-type R_3NiSi_3 (R=Gd–DY) compounds

A.V. Morozkin [a,*], V.O. Yapaskurt [b], R. Nirmala [c], S.K. Malik [d], S. Quezado [d], Jinlei Yao [e], Y. Mozharivskyj [e], A.K. Nigam [f], O. Isnard [g,h]

[a] Department of Chemistry, Moscow State University, Leninskie Gory, House 1, Building 3, GSP-2, Moscow 119992, Russia
[b] Department of Petrology, Faculty of Geology, Moscow State University, Leninskie Gory, Moscow 119992, Russia
[c] Indian Institute of Technology Madras, Chennai 600036, India
[d] Departamento de Física Teórica e Experimental, Universidade Federal do Rio Grande do Norte, Natal 59082-970, Brazil
[e] Department of Chemistry and Chemical Biology, McMaster University, 1280 Main Street West, Hamilton, Ontario, Canada L8S 4M1
[f] Tata Institute of Fundamental Research, Mumbai 400005, India
[g] Université Grenoble Alpes, Inst NEEL, BP166, F-38042 Grenoble, France
[h] CNRS, Institut NEEL, 25 rue des martyrs, F-38042 Grenoble, France

ARTICLE INFO

Article history:
Received 6 February 2015
Received in revised form
27 August 2015
Accepted 7 September 2015
Available online 9 September 2015

Keywords:
Rare-earth compounds
Magnetic properties
Neutron diffraction
Magnetic structure

ABSTRACT

Magnetic measurements and neutron powder diffraction investigations on the Y_3NiSi_3-type R_3NiSi_3 compounds (R=Gd, Tb, Dy) reveal their complex antiferromagnetic ordering. Magnetic measurements on Gd_3NiSi_3, Tb_3NiSi_3 and Dy_3NiSi_3 indicate antiferromagnetic-like transition at temperatures 260 K, 202 K and 140 K, respectively. Also, the Tb_3NiSi_3 and Dy_3NiSi_3 compounds show spin-reorientation transition at 132 K and 99 K, respectively. Below the spin-reorientation transition, the isothermal magnetization curves indicate the metamagnetic-like behavior of Tb_3NiSi_3 and Dy_3NiSi_3. The magnetocaloric effect of Dy_3NiSi_3 is calculated in terms of isothermal magnetic entropy change and it reaches a maximum value of -1.2 J/kg K and -1.1 J/kg K for a field change of 50 kOe near 146 K and 92 K, respectively. The neutron diffraction studies of Tb_3NiSi_3 suggest the magnetic ordering of the Tb2 4*j* sublattice and no magnetic ordering of the Tb1 2*a* sublattice. Tb_3NiSi_3 transforms from the high temperature paramagnetic state to the commensurate high-temperature *a*- and *c*-axis antiferromagnet of **I′2/m** magnetic space group below 250 K. Below 150 K, the high-temperature antiferromagnet transforms into the low-temperature *a*-, *b*- and *c*-axis antiferromagnet of **I′i** magnetic space group. At 1.5 K, the terbium magnetic moment in Tb2 sublattice and its *a*-, *b*- and *c*-axis components reach the values of M_{Tb2}=8.2(1) μ_B, M_{aTb2}=5.9(1) μ_B, M_{bTb2}=4.3(2) μ_B and M_{cTb2}=3.7(2) μ_B, respectively.

1. Introduction

Recently, the Y_3NiSi_3-type R_3NiSi_3 compounds (R=Y, La–Sm, Gd–Dy) were synthesized and their crystal structures were determined by Merlo and coworkers [1]. The Y_3NiSi_3-type structure (space group *Immm*, No. 71) is the ordered variant of the Ta_3B_4-type structure [2,3]. The relationship between their structures and physical properties needs a systematic study. This work aims to understand the magnetic ordering of Y_3NiSi_3-type {Gd, Tb, Dy}$_3NiSi_3$ compounds via magnetization and neutron diffraction studies.

2. Materials and methods

The '{Gd, Tb, Dy}$_3NiSi_3$' alloys were prepared by arc melting of the stoichiometric amounts of rare earth (99.9 wt%), Ni (99.95 wt%) and Si (99.99 wt%). The samples were annealed at 1070 K for 240 h in an argon-filled and sealed quartz tube and subsequently quenched in ice-cold water. The structure, purity and composition of the polycrystalline sample were evaluated using powder X-ray diffraction and electron microprobe analysis. The X-ray data were obtained on a Rigaku D/MAX-2500 diffractometer ($CuK_{\alpha1}$ radiation, 2θ=10–80°, step 0.02°, 1 s/step). An INCA-Energy-350 X-ray EDS spectrometer (Oxford Instruments) on the Jeol JSM-6480LV scanning electron microscope (20 kV accelerating voltage, beam current 0.7 nA and beam diameter 50 μm) was employed to perform the microprobe analyses of the sample. Signals from three points were averaged and estimated standard deviations were 1 at% for rare earth (measured by L-series lines), 1 at% for Ni and 1 at% for Si (measured by K-series lines).

The magnetization of the polycrystalline '{Gd, Tb, Dy}$_3NiSi_3$' alloys (mass ~0.01 g) was measured on a commercial MPMS SQUID magnetometer (Quantum Design)) and using the VSM option of the Dynacool, PPMS (Quantum Design) in the temperatures range of 2–300 K

* Corresponding author.
E-mail address: morozkin@tech.chem.msu.ru (A.V. Morozkin).

http://dx.doi.org/10.1016/j.jmmm.2015.09.035
0304-8853/

in fields up to 70 kOe and 140 kOe.

Neutron diffraction experiments were carried out at the high flux reactor of the Institut Laue Langevin (Grenoble, France). The data were collected in a zero magnetic field on the two-axis D1B powder diffractometer equipped with a 1300 cell curved detector spanning the 2θ range of 130° [4]. The temperature ranges were 250–1.5 K with a step of ~20 K. The neutron wavelength of 2.524 Å was selected by the (002) reflection of a pyrolitic graphite monochromator and the 2θ step was 0.1°.

3. Theory/calculations

The unit cell data were derived from the powder XRD using the Rietan program [5,6] in the isotropic approximation at room temperature. The paramagnetic susceptibility was fitted to Curie–Weiss law and the effective magnetic moments and paramagnetic Curie temperatures were obtained [7]. Magnetocaloric effect (MCE) is calculated in terms of the isothermal magnetic entropy change, ΔS_m, using the magnetization vs field data obtained near the magnetic transition using the thermodynamic Maxwell equation [8]. The neutron diffraction data were refined with the FULLPROF program [9]. The magnetic space groups [10–11] were used for the analysis of neutron diffraction data.

4. Results

4.1. Crystal structure

Both the microprobe and X-ray powder analyses showed that '{Gd, Tb, Dy}$_3$NiSi$_3$' alloys contain about 77–85 wt% of Y_3NiSi_3-type R_3NiSi_3, 6–9 wt% of FeB- or CrB-type *R*Si [2,3] and 9–14 wt% of AlB_2-type ~RNi_xSi_{2-x} [2,3] phases (see for example, the microstructure of 'Tb_3NiSi_3' alloy in Fig. 1). The sample compositions and refined lattice parameters of Y_3NiSi_3-type {Gd, Tb, Dy}$_3$NiSi$_3$ are given in Table 1.

The atomic sites and interatomic distances of Y_3NiSi_3-type Tb_3NiSi_3 are given in Table 2. The shortest interatomic distances are close to the sum of metallic radii of corresponding elements [12,13], which is indicative of a metallic type bonding in Tb_3NiSi_3. Formally, the shortest Tb1-Tb1, Tb1-Tb2 and Tb2-Tb2 distances facilitate the magnetic ordering of Tb2 sublattice and they preclude the magnetic ordering of Tb1 sublattice in Tb_3NiSi_3.

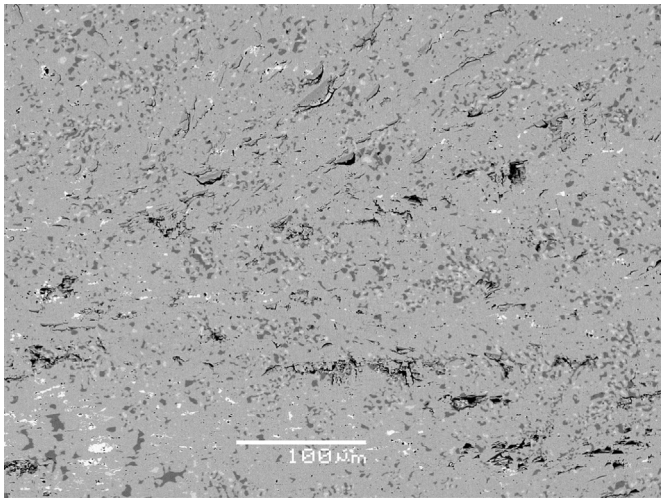

Fig. 1. Microstructure of 'Tb_3NiSi_3' alloy after annealing at 1070 K for a 240 h: '$Tb_{44}Ni_{14}Si_{42}$' (Y_3NiSi_3-type) (gray), '$Tb_{51}Si_{49}$' (CrB-type) (white) and '$Tb_{34}Ni_{21}Si_{45}$' (AlB_2-type) (black-gray). The black sites are defects of sample's surface.

Table 1
Unit cell data of Y_3NiSi_3-type R_3NiSi_3 compounds (*R*=Gd, Tb and Dy) (space group *Immm*, N 71, *o*I14) The sample's compositions are given in bottom of Table.

N	Compound	*a*(nm)	*b*(nm)	*c*(nm)$^-$	R_F (%)	Refs.
1	Gd_3NiSi_3	0.3983	0.4158	1.7554		[1]
	Gd_3NiSi_3[a]	0.39796(6)	0.41569(7)	1.7551(2)	5.3	d
2	Tb_3NiSi_3	0.3959	0.4126	1.7427		[1]
	Tb_3NiSi_3[b]	0.39567(2)	0.41217(2)	1.74059(9)	4.4	d
3	Dy_3NiSi_3	0.3946	0.4106	1.7339		[1]
	Dy_3NiSi_3[c]	0.39472(3)	0.41044(4)	1.7337(1)	2.7	d

[a] sample contains 77 wt% of Y_3NiSi_3-type Gd_3NiSi_3, 9 wt% of FeB-type GdSi and 14 wt% of AlB_2-type $Gd_{34}Ni_{21}Si_{45}$ phases;
[b] sample contains 85 wt% of Y_3NiSi_3-type Tb_3NiSi_3, 6 wt% of CrB-type TbSi and 9 wt% of AlB_2-type $Tb_{34}Ni_{23}Si_{43}$ phases;
[c] sample contains 82 wt% of Y_3NiSi_3-type Dy_3NiSi_3, 8 wt% of CrB-type DySi and 10 wt% of AlB_2-type $Dy_{34}Ni_{27}Si_{39}$ phases;
[d] this work.

Table 2
Interatomic distances of Y_3NiSi_3-type Tb_3NiSi_3: space group *Immm*, N 71, *o*I14, *a*=0.39567(2) nm, *b*=0.41217(2) nm, *c*=1.74059(9) nm, *Z*=2, Tb1 (2*a*) [0, 0, 0], Tb2 (4*j*) [1/2, 0, 0.1847(2)], *M*=$Ni_{0.5}Si_{0.5}$ (4*i*) [0, 0, 0.5648(5)], Si (4*j*) [1/2, 0, 0.3623(9)], R_F=4.4% (at 298 K) (ESD ± 0.0005). In the Table are given the ratio of interatomic distances to the sum of the atomic radii of the corresponding elements Δ=D/(r_{atom1}+r_{atom2}) (r_{Tb}=0.17788 nm, r_{Ni}=0.12459 nm, r_{Si}=0.1176 nm, r_M=0.5•r_{Si} +0.5•r_{Ni}=0.12109 nm) [12,13]) and coordination numbers δ. The shortest Tb1-Tb1, Tb2-Tb2 and Tb1-Tb2 distances are selected by a bold character.

Atom	-Atom	D (nm)	Δ	Atom	-Atom	D (nm)	Δ
Tb1-	8*M*	0.3071	1.02	M-	1*M*	0.2256	0.93
	4Si	0.3161	1.07		2Si	0.2350	0.98
	4Tb2	**0.3775**	**1.06**		2Tb2	0.2933	0.98
	2Tb1	**0.39567**[a]	**1.11**		4Tb1	0.3071	1.03
		δ=16				**δ=9**	
Tb2-	2*M*	0.2933	0.98	Si -	2*M*	0.2350	0.98
	4Si	0.2972	1.01		4Tb2	0.2972	1.01
	1Si	0.3091	1.05		1Tb2	0.3091	1.05
	4Tb2	**0.3651**	**1.03**		2Tb1	0.3161	1.07
	2Tb1	**0.3775**	**1.06**			**δ=9**	
	2Tb2	0.39567[a]	1.11				
		δ=15					

[a] interatomic distance equals the *a* cell parameter of unit cell.

4.2. Magnetic transitions

Magnetization and inverse magnetic susceptibility of '{Gd, Tb, Dy}$_3$NiSi$_3$' alloys are shown in Fig. 2 as a function of temperature. The 'Gd_3NiSi_3', 'Tb_3NiSi_3' and 'Dy_3NiSi_3' exhibit antiferromagnetic-like transitions at 260 K, 202 K and 140 K, respectively. Also, 'Tb_3NiSi_3' and 'Dy_3NiSi_3' show possible spin-reorientation transitions at 132 K and 99 K, respectively. In addition, there is an anomaly in the magnetization data at low temperatures (as marked in the figures) of these samples that almost conicide with Néel points of FeB-type GdSi (55 K) [14], CrB-type TbSi (56 K) [15] and DySi (43 K), respectively [15].

The AlB_2-type $GdSi_{1.65}$, $TbSi_{1.7}$ and, $DySi_{1.6}$ compounds are known to exhibit antiferromagnetic transition at 33 K, 32 K and 17 K, respectively [16,17]. Certainly, the Néel points of AlB_2-type {Gd, Tb, Dy}Ni_xSi_{2-x} solid solutions should somewhat differ from the initial AlB_2-type {Gd, Tb, Dy}Si_{2-x}. However, no anomalies were observed in the magnetization data of '{Gd, Tb, Dy}$_3$NiSi$_3$' alloys that may correspond to the admixture AlB_2-type {Gd, Tb, Dy}Ni_xSi_{2-x} phases.

The paramagnetic susceptibility of 'Gd_3NiSi_3', 'Tb_3NiSi_3' and 'Dy_3NiSi_3' follows Curie–Weiss law in the temperature range of ~270–300 K, ~220–300 K and ~160–300 K, respectively (Insets in Fig. 2). The fit to the Curie–Weiss law yields positive paramagnetic Weiss temperatures Θ_p of 150 K, 133 K and 74 K which

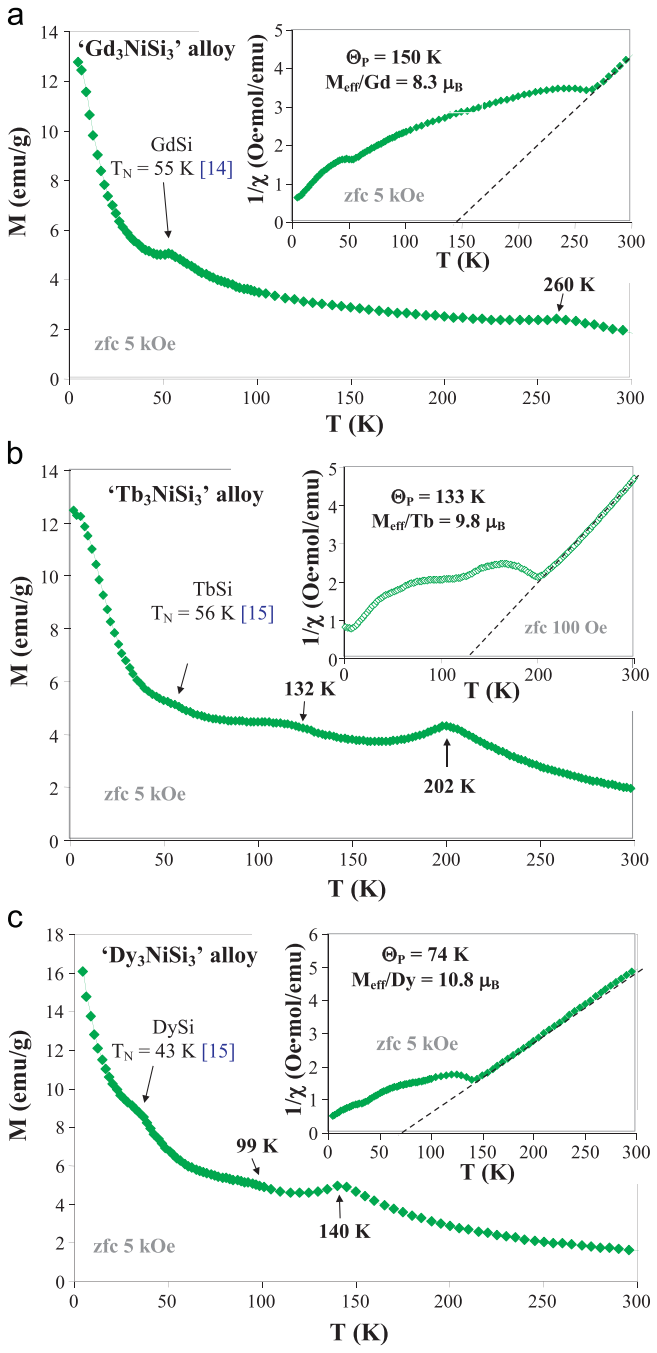

Fig. 2. Magnetization and inverse magnetic susceptibility as a function of temperature of (a) 'Gd$_3$NiSi$_3$', (b) 'Tb$_3$NiSi$_3$' and (c) 'Dy$_3$NiSi$_3$' alloys.

indicate dominant ferromagnetic or mixed ferromagnetic–antiferromagnetic interactions in these compounds. The effective paramagnetic moment values per formula unit (M_{eff}/fu) are 14.4 μ_B, 16.9 μ_B and 18.7 μ_B respectively and effective paramagnetic moments per rare earth are 8.3 μ_B, 9.8 μ_B and 10.8 μ_B respectively, for the 'Gd$_3$NiSi$_3$', 'Tb$_3$NiSi$_3$' and 'Dy$_3$NiSi$_3$' samples. These values are slightly larger than the theoretical effective paramagnetic moment of trivalent Gd (7.94 μ_B), Tb (9.72 μ_B) and Dy (10.65 μ_B) [17]. The magnetization data suggest that the high-temperature transitions be attributed to the ordering of Y$_3$NiSi$_3$-type Gd$_3$NiSi$_3$, Tb$_3$NiSi$_3$ and Dy$_3$NiSi$_3$ compounds, whereas the low-temperatures anomaly in magnetization curves are results of magnetic ordering of {Gd, Tb, Dy}Si admixture phases. In contrast, the Gd$_3$NiSi$_3$, Tb$_3$NiSi$_3$ and Dy$_3$NiSi$_3$ compounds show a low-temperature transition. The temperatures of magnetic transitions of Tb$_3$NiSi$_3$ and Dy$_3$NiSi$_3$ correspond to de Gennes rule [17], which indicate their same magnetic ordering (Table 3). Meantime, the magnetic ordering of Gd$_3$NiSi$_3$ should be differs from the ordering of Tb$_3$NiSi$_3$ and Dy$_3$NiSi$_3$ from de Gennes rule [17].

4.3. Magnetization and magnetocaloric effect

The magnetization vs field data of 'Tb$_3$NiSi$_3$' show a linear behavior at 150 K as expected in the antiferromagnetic state (Fig. 3a). However, the magnetization undergoes a complex field induced transition at 25 K and 5 K and shows a tendency to saturate. A magnetic moment of 8.4 μ_B/fu in 70 kOe at 5 K is obtained and is less than the theoretical ordered state moment of Tb being 9 μ_B [17]. This suggests a possible non-collinear magnetic order in Tb$_3$NiSi$_3$ below temperature of spin-reorientation transition (T_{SR} = 132 K). 'Tb$_3$NiSi$_3$' shows a broad metamagnetic transition at 25 K and 5 K in critical fields of 20 kOe and 30 kOe, respectively (Figs. 3a and b).

The magnetization vs field of Dy$_3$NiSi$_3$ has similar behavior as that of Tb$_3$NiSi$_3$ (Fig. 3c). The magnetization of 'Dy$_3$NiSi$_3$' is linear in temperature below antiferromagnetic ordering temperature (T_N = 140 K) at 100 K and exhibits a field induced transition in critical field fo ~27 kOe at 2 K below the spin-reorientation transition (T_{SR}=99 K). Even in field of 140 K at 2 K, the saturation magnetization of Dy$_3$NiSi$_3$ is only 7.3 μ_B/Dy (22 μ_B/fu), while the theoretical moment of trivalent Dy is 9 μ_B [17].

The magnetocaloric effect of 'Dy$_3$NiSi$_3$' is calculated from magnetization vs magnetic field data in terms of the isothermal magnetic entropy change (ΔS_m) and it reaches a maximum values of −1.2 J/kg K and −1.1 J/kg K for a field change of 50 kOe around Néel point at 146 K and temperature of spin re-orientation transition at 92 K of Dy$_3$NiSi$_3$, respectively (Fig. 4). These ΔS_m values are close to the to the calculated magnetocaloric effect of single phase Dy$_3$NiSi$_3$ for a field change of 50 kOe: ΔS_m^{calc} ~ −1.5 J/kg K at 146 K and ΔS_m^{calc} ~ −1.3 J/kg K at 92 K (here $\Delta S_m^{calc} = \Delta S_m / m_{Dy3NiSi3}$ and $m_{Dy3NiSi3}$ the mass fraction of Y$_3$NiSi$_3$-type

Table 3
Magnetic properties of Y$_3$NiSi$_3$-type {Gd, Tb, Dy}$_3$NiSi$_3$: paramagnetic temperature Θ_P, effective magnetic moments per rare earth atom M_{eff}/R, temperature of antiferromagnetic (T_N) and spin-reorientation (T_{SR}) transitions, saturation magnetization per formula unit M_{sat}/fu, critical field H_c and magnetocaloric effect (MCE) in terms of isothermal magnetic entropy change, ΔS_m.

Compound	Θ_P (K)	M_{eff}/R (μ_B)	T_N (K)	T_{SR} (K)	M_{sat}/R (μ_B)	H_c (kOe)	ΔS_m (J/kg K) 0–20 kOe	ΔS_m (J/kg K) 0–50 kOe
Gd$_3$NiSi$_3$	150	8.2	260	–				
Tb$_3$NiSi$_3$	133	9.8	202	132	10.1 (25 K, 70 kOe) 9.9 (5 K, 70 kOe)	20 (25 K) 30 (5 K)		
Dy$_3$NiSi$_3$	74	10.8	140	99	22 (2 K, 140 kOe)	27 (2 K)	−0.4 (146 K) [a] −0.4 (92 K) [a]	−1.2 (146 K) [a] −1.1 (92 K) [a]

[a] magnetic entropy change of'Dy$_3$NiSi$_3$' alloy.

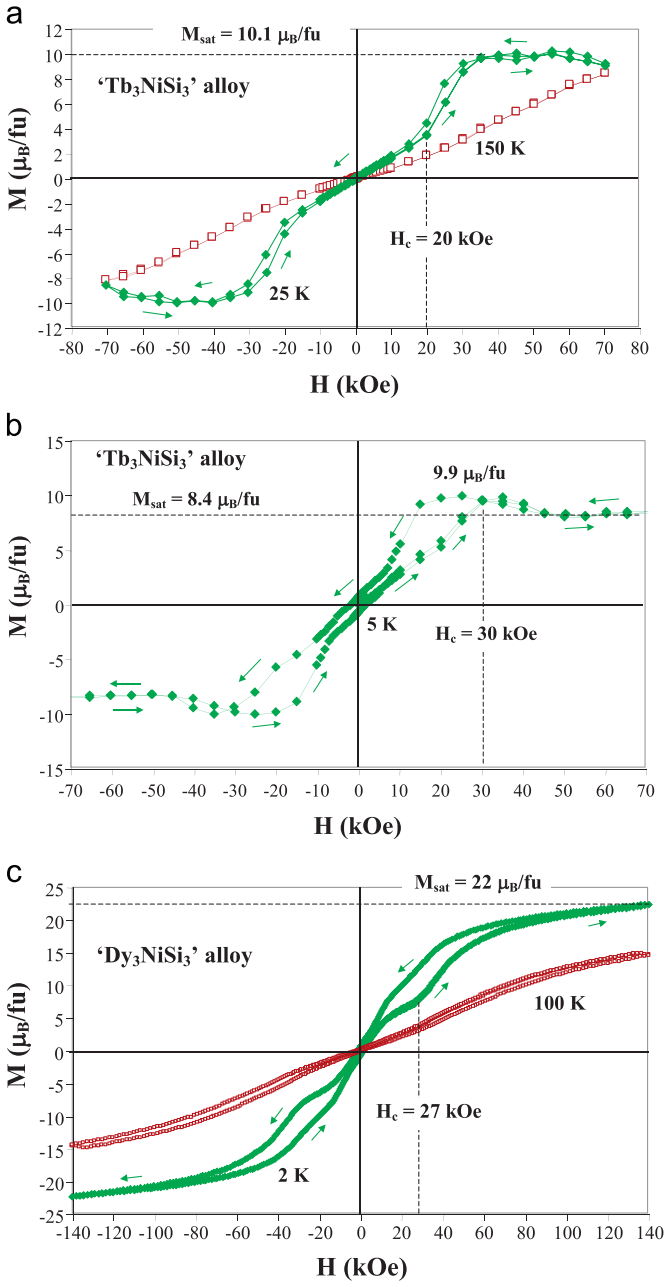

Fig. 3. Magnetization vs magnetic field of (a) 'Tb_3NiSi_3' at 150 K and 25 K, (b) 'Tb_3NiSi_3' at 5 K and (c) 'Dy_3NiSi_3' at 100 K and 2 K.

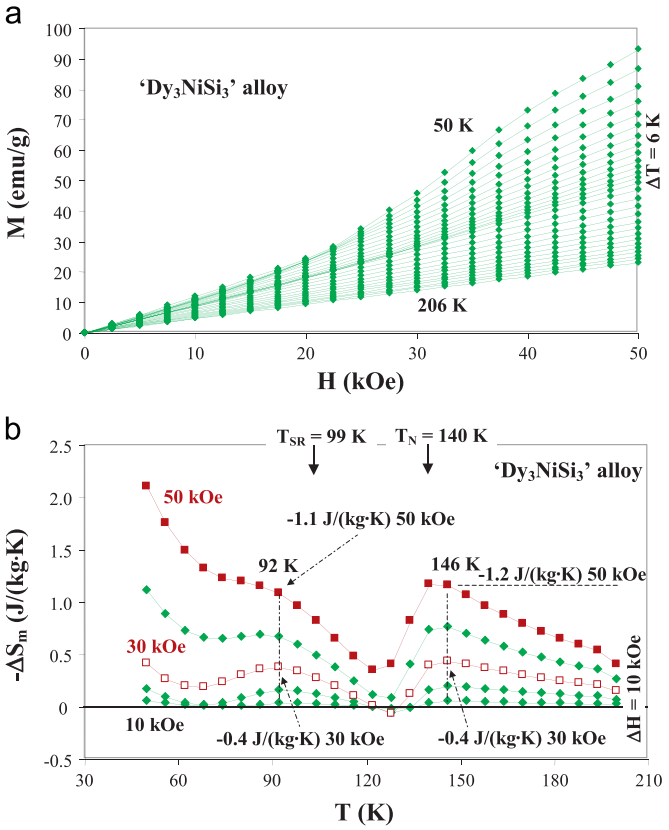

Fig. 4. (a) Magnetization-field isotherms from 50 K to 206 K and (b) the isothermal magnetic entropy change, $-\Delta S_m$ vs temperature of "Dy_3NiSi_3' alloy.

Dy_3NiSi_3 that given in Table 1). Thus the role of minority phases in the estimated magnetocaloric effect values seems to be weak and within the error bar of estimated values of ΔS_m.

The magnetic data of {Gd, Tb, Dy}$_3$NiSi$_3$ compounds are summarized in Table 3.

4.4. *Magnetic structure of Tb_3NiSi_3*

At 250 K, the neutron diffraction patterns of Tb_3NiSi_3 in zero applied field correspond to the paramagnetic state. At 180 K and down to 125 K, a set of commensurate magnetic reflections with a $\mathbf{K}_0$=[0, 0, 0] propagation vector appear indicating the magnetic ordering of Tb_3NiSi_3 (Figs. 5**a** and 5**b**). From 125 K to 1.5 K, a set of additional commensurate magnetic reflections with a $\mathbf{K}_0$=[0, 0, 0] shows transformation of magnetic structure of Tb_3NiSi_3 (Fig. 5**c**). The ordering temperatures found from the neutron diffraction study (between 250 K and 180 K and between 150 K and 125 K) are in good agreement with the values deduced from the magnetization measurements of T_N=202 K and T_{SR}=132 K (Fig. 6**a**).

The atomic positions for the Tb1 *2a* and Tb2 *4j* sites in the *Immm* space group with the corresponding symmetry operators are given in Table 4.

Analysis of neutron diffraction patterns at 180 K, 170 K and 150 K shows that antiferromagnetic ordering of **I′2/m** magnetic space group (high-temperature HT **Antiferromagnet**) has the best agreement with experiment: magnetic structure of Tb_3NiSi_3 consists of non-magnetically ordered Tb1 sublattice and magnetically ordered Tb2 sublattice as a set of *a*-axis antiferromagnetic $\mathbf{AF}_a$ and *c*-axis antiferromagnetic $\mathbf{AF}_c$ components of **I′2/m**={**1**, $\mathbf{m}_y$}×{**1**, **i**}×{**1**, **1**′/[1/2, 1/2, 1/2]} magnetic space group and propagation vector $\mathbf{K}_0$=[0, 0, 0] (Table 4 and Figs. 7a and b).

Between 150 K and 125 K, the Tb_3NiSi_3 exhibits reorientation transition with decreasing of magnetic symmetry down to triclinic magnetic space group **I′i**={**1**, **i**}×{**1**, **1**′/[1/2, 1/2, 1/2]}: magnetic structure of Tb_3NiSi_3 (LT **Antiferromagnet**) consists of non-magnetic Tb1 sublattice and magnetically ordered Tb2 sublattice as a set of *a*-, *b*- and *c*-axis antiferromagnetic components $\mathbf{AF}_a$, $\mathbf{AF}_b$ and $\mathbf{AF}_c$ of **I′i** magnetic space group and $\mathbf{K}_0$=[0, 0, 0] (Table 4, Figs. 7c and d).

Attempt to refine the magnetic structure of Tb_3NiSi_3 with magnetic ordering of Tb1 sublattice was not satisfactory in the present work.

At 50 K, the set of magnetic reflections of CrB-type TbSi are observed in neutron diffraction pattern and at 1.5 K the TbSi exhibits the antiferromagnetic ordering with **K**=[1/2, 0, 1/2] propagation vector [15].

The model with known magnetic structure of TbSi [15] and LT **Antiferromagnet** of the Tb_3NiSi_3 has best agreement with neutron diffraction patterns at 50 K and down to 1.5 K (Fig. 5d). The

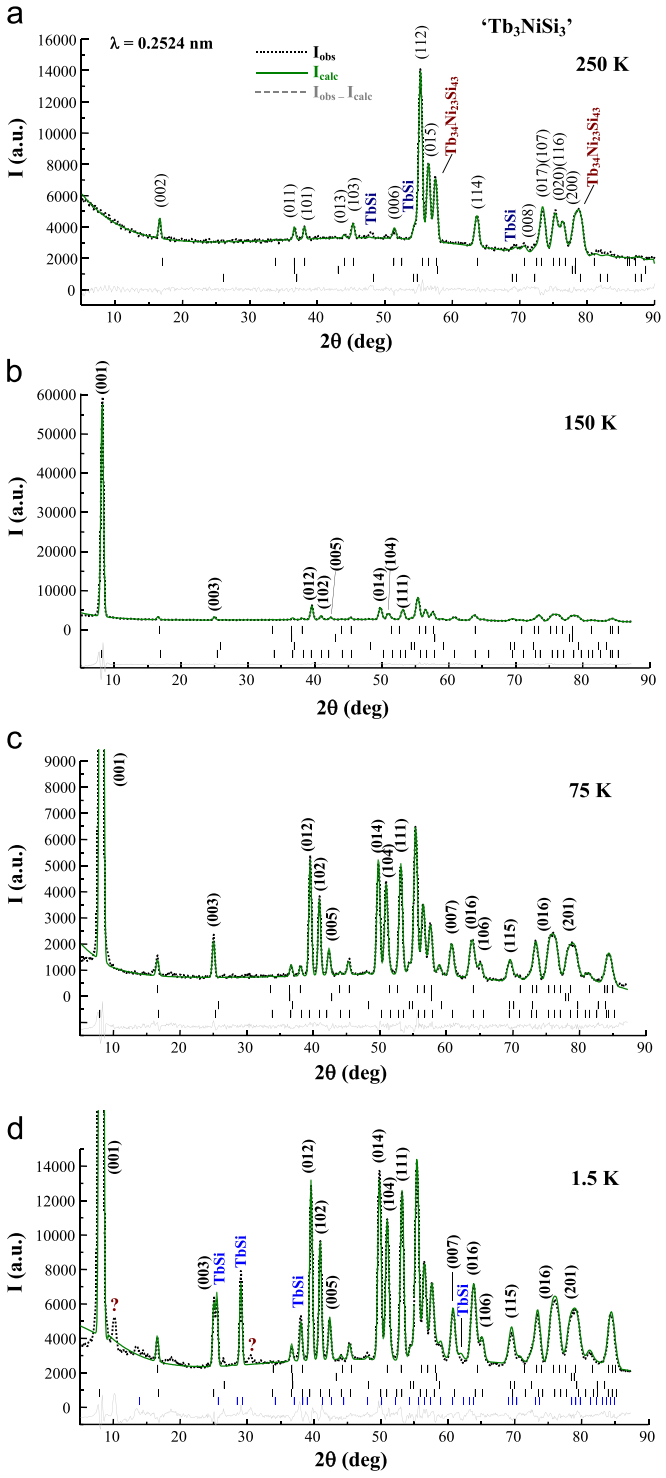

Fig. 5. Neutron diffraction patterns of'Tb_3NiSi_3' alloy (a) at 250 K (paramagnetic state), (b) at 150 K: the Tb_3NiSi_3 is the *a*- and *b*-axis high-temperature HT **Antiferromagnet** with $\mathbf{K}_0$=[0, 0, 0] wave vector, (c) at 75 K: Tb_3NiSi_3 is the *a*-, *b*- and *c*-axis low-temperature LT **Antiferromagnet** with $\mathbf{K}_0$=[0, 0, 0] wave vector and (d) at 1.5 K: Tb_3NiSi_3 is the *a*-, *b*- and *c*-axis low-temperature LT **Antiferromagnet** with $\mathbf{K}_0$=[0, 0, 0] wave vector and TbSi is antiferromagnet with $\mathbf{K}$=[1/2, 0, 1/2] wave vector. The first, second and third rows of ticks refer to the nuclear Bragg peaks of Y_3NiSi_3-type Tb_3NiSi_3, AlB_2-type $Tb_{34}Ni_{23}Si_{46}$ and CrB-type TbSi, respectively (the strongest nuclear reflections of $Tb_{34}Ni_{23}Si_{43}$ and TbSi are shown in Fig. 4a). The fourth and fifth rows of lines refer to the magnetic reflections of Tb_3NiSi_3 and TbSi, respectively. The (hkl) of strongest magnetic reflections of Tb_3NiSi_3 are indicated in Figs. 5b–d. The strongest magnetic reflections of TbSi are marked in Fig. 5d.

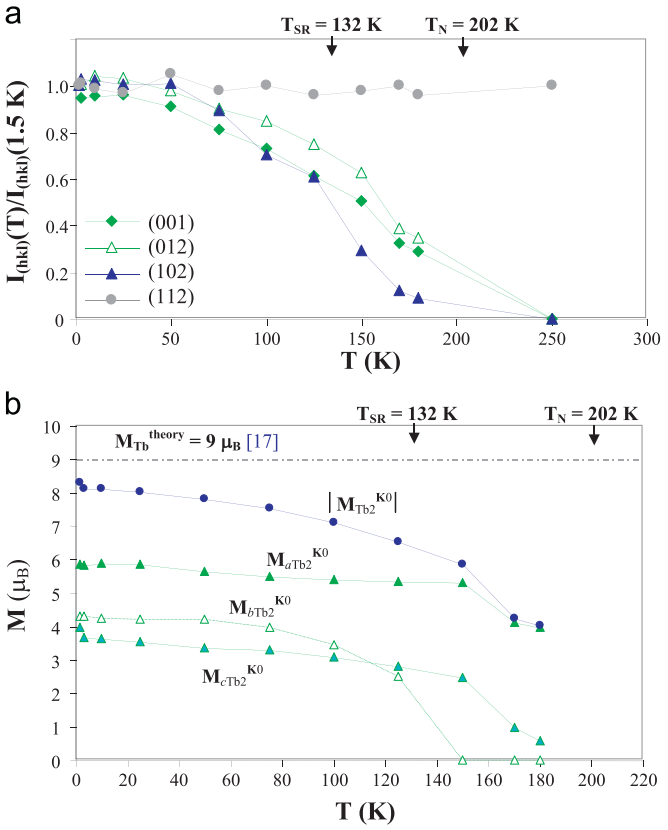

Fig. 6. Thermal evolution of (a) strongest magnetic reflections $I_{(hkl)}$ in the neutron diffraction patterns of Tb_3NiSi_3 and (b) $\mathbf{M}_{a\mathrm{Tb2}}^{\mathbf{K0}}$, $\mathbf{M}_{b\mathrm{Tb2}}^{\mathbf{K0}}$ and $\mathbf{M}_{c\mathrm{Tb2}}^{\mathbf{K0}}$ the Tb2 magnetic moments along *a*, *b* and *c* axis, respectively and $|\mathbf{M}_{\mathrm{Tb2}}^{\mathbf{K0}}|$ the resulting magnitude of terbium magnetic moment with $\mathbf{K}_0$=[0, 0, 0]. The temperatures of magnetic transition detected from magnetic measurements are shown in **Figure**.

set of unindexed reflections may belong to the weak incommensurate antiferromagnetic component of Tb_3NiSi_3. The magnetic ordering of AlB_2-type $Tb_{34}Ni_{23}Si_{43}$ was not detected in present work.

Meanwhile, the magnitude of terbium magnetic moment at 1.5 K with $\mathbf{K}_0$ propagation vector of 8.2(1) μ_B is close to magnetic moment of pure terbium M_{Tb}^{theory}=9 μ_B [17], which indicates the most crucial role of antiferromagnetic commensurate component in magnetic ordering of Tb_3NiSi_3.

Thermal evolution of values of the *a*-axis antiferromagnetic $\mathbf{AF}_a$, *b*-axis antiferromagnetic $\mathbf{AF}_b$ and *c*-axis antiferrromagnetic $\mathbf{AF}_c$ components and resulting terbium magnetic moment are shown in Fig. 6b. The magnetic components and unit cell data of Tb_3NiSi_3 are listed in Table 5.

It is worth to point out that no significant ordered magnetic moment has been found on the Ni site.

Thus, below the antiferromagnetic ordering temperature of T_N =202 K and until the temperature of spin-reorintation transition T_{SR}=132 K, the Tb_3NiSi_3 compound exhibits antiferromagnetic ordering of Tb2 sublattice: paramagnet→HT **Antiferromagnet** $(\mathbf{AF}_a+\mathbf{AF}_c)^{\mathbf{K0}}\mathbf{I'2/m}$. Below 150 K and below T_{SR}=132 K the HT **Antiferromagnet** transforms to the LT **Antiferromagnet** with decrease of magnetic symmetry in to magnetic space group **I′i**: HT **Antiferromagnet** $(\mathbf{AF}_a+\mathbf{AF}_c)^{\mathbf{K0}}$ **I′2/m**→LT **Antiferromagnet** $(\mathbf{AF}_a+\mathbf{AF}_b+\mathbf{AF}_c)^{\mathbf{K0}}$ **I′i**. Due to specific structural features of terbium sublattice and magnetic ordering of Tb2 sublattice, the Tb1 sublattice does not show any magnetic order in Tb_3NiSi_3. and the atoms of Tb2 sublattice that are neighbors to the Tb1 atoms are antiferromagnetically ordered (see for example, the cluster $Tb1^2$-$2Tb2^3$ and $2Tb2^4$ atoms in Fig. 7a).

Table 4
Atomic positions of the terbium Tb1 2*a* and Tb2 4*j* site of space group *Immm* and commensurate magnetic component of corresponding terbium atoms (retained by Tb_3NiSi_3 compound) with the symmetry operators (the $\mathbf{m}_a$. $\mathbf{m}_b$ and $\mathbf{m}_c$ are *a*-, *b*- and *c*-axis commensurate magnetic component).

				Immm[a]	HT AF: I′2/m[c]			LT AF: I′i[d]		
Atom	**x/*a***	**y/*b***	**z/*c***	Symmetry operator	$\mathbf{m}_a$	$\mathbf{m}_b$	$\mathbf{m}_c$	$\mathbf{m}_a$	$\mathbf{m}_b$	$\mathbf{m}_c$
$Tb1^1$	0	0	0	*Pmmm*[b]	0	0	0	0	0	0
$Tb1^2$	1/2	1/2	1/2	*Pmmm*/[1/2, 1/2, 1/2]	0	0	0	0	0	0
$Tb2^1$	1/2	0	z	{**1**, $\mathbf{m}_x$, $\mathbf{m}_y$, $\mathbf{2}_z$}	+	0	+	+	+	+
$Tb2^2$	1/2	0	−z	{**i**, $\mathbf{2}_x$, $\mathbf{2}_y$, $\mathbf{m}_z$}	−	0	−	−	−	−
$Tb2^3$	0	1/2	1/2+z	{**1**/[1/2, 1/2, 1/2], $\mathbf{m}_x$/[1/2, 1/2, 1/2], $\mathbf{m}_y$/[1/2, 1/2, 1/2], $\mathbf{2}_z$/[1/2, 1/2, 1/2]}	−	0	−	−	−	−
$Tb2^4$	0	1/2	1/2−z	{**i**/[2, 1/2, 1/2], $\mathbf{2}_x$/[1/2, 1/2, 1/2], $\mathbf{2}_y$/[1/2, 1/2, 1/2], $\mathbf{m}_z$/[1/2, 1/2, 1/2]}	+	0	+	+	+	+

[a] *Immm* (x, y, z)={**1**, $\mathbf{m}_x$, $\mathbf{m}_y$, $\mathbf{2}_z$, **i**, $\mathbf{2}_x$, $\mathbf{2}_y$, $\mathbf{m}_z$, **1**/[1/2, 1/2, 1/2], $\mathbf{m}_x$/[1/2, 1/2, 1/2], $\mathbf{m}_y$/[1/2, 1/2, 1/2], $\mathbf{2}_z$/[1/2, 1/2, 1/2], **i**/[1/2, 1/2, 1/2], $\mathbf{2}_x$/[1/2, 1/2, 1/2], $\mathbf{2}_y$/[1/2, 1/2, 1/2], $\mathbf{m}_z$/[1/2, 1/2, 1/2]}={**1**, $\mathbf{m}_x$}×{**1**, $\mathbf{m}_y$}×{**1**, **i**}×{**1**, **1**/[1/2, 1/2, 1/2]}.
[b] *Pmmm* (x, y, z)={**1**, $\mathbf{m}_x$, $\mathbf{m}_y$, $\mathbf{2}_z$, **i**, $\mathbf{2}_x$, $\mathbf{2}_y$, $\mathbf{m}_z$}={**1**, $\mathbf{m}_x$}×{**1**, $\mathbf{m}_y$}×{**1**, **i**}.
[c] **I′2/m**={**1**, $\mathbf{m}_y$}×{**1**, **i**}×{**1**, **1′**/[1/2, 1/2, 1/2]}.
[d] **I′i**={**1**, **i**}×{**1**, **1′**/[1/2, 1/2, 1/2]}.

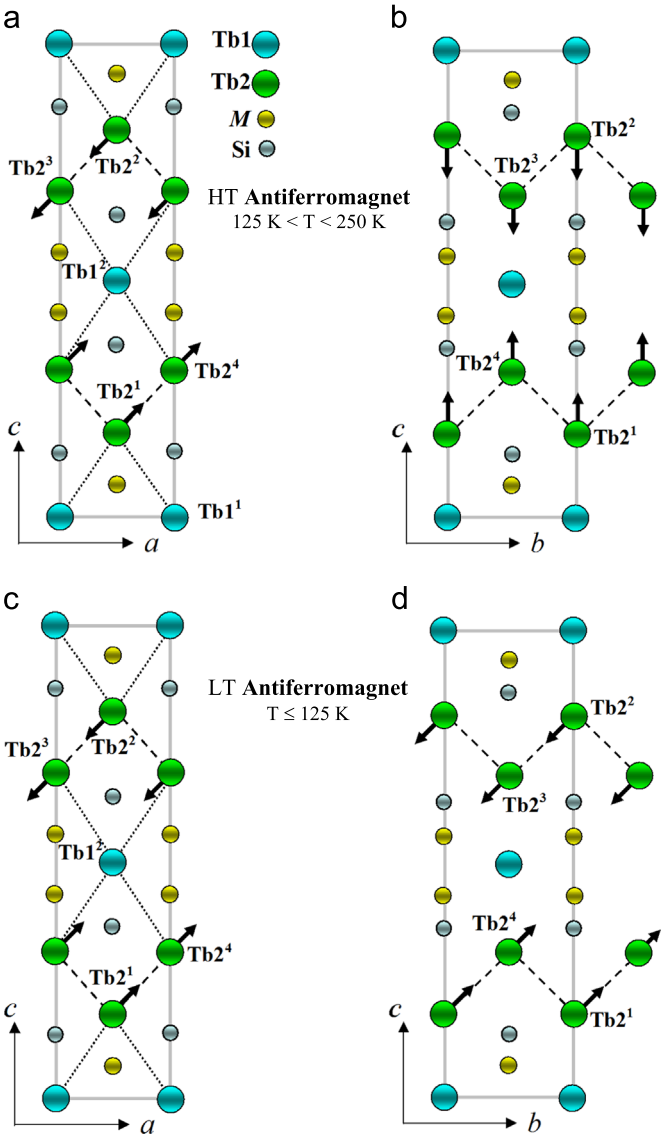

Fig. 7. The magnetic ordering of Y_3NiSi_3-type Tb_3NiSi_3: (a), (b) high-temperature HT **Antiferromagnet** with *a*-axis antiferromagnetic $\mathbf{AF}_a$ and *c*-axis antiferromagnetic $\mathbf{AF}_c$ components of **I′2/m** magnetic space group of $\mathbf{K}_0$ wave vector: $(\mathbf{AF}_a+\mathbf{AF}_c)^{\mathbf{K0}}$ **I′2/m** $\mathbf{K}_0$=[0, 0, 0] and (c), (d) low-temperature LT **Antiferromagnet** with *a*-, *b*- and *c*-axis antiferromagnetic components $\mathbf{AF}_a$, $\mathbf{AF}_b$ and $\mathbf{AF}_c$ of **I′i** magnetic space group of $\mathbf{K}_0$ wave vector: $(\mathbf{AF}_a+\mathbf{AF}_b+\mathbf{AF}_c)^{\mathbf{K0}}$ **I′i** $\mathbf{K}_0$=[0, 0, 0]. The shortest Tb1-Tb1, Tb1-Tb2 and Tb2-Tb2 interatomic distances are shown in Figures a and c. The magnetic moment of terbium in Tb1 sublattice is zero.

5. Discussion

We suggest that due to specific features of rare earth sublattice the Y_3NiSi_3-type R_3NiSi_3 (R=Gd, Tb and Dy) compounds exhibit magnetic ordering of only the *R*2 4*j* sublattice and the {Gd, Tb, Dy)$_3NiSi_3$ compouns show the positive value of paramagnetic Weiss temperature in spite of the observed antiferromagnetic ordering. This obviously indicates the presence of competing magnetic interactions. Indeed, on the one hand ferromagnetic coupling is observed within the Tb2 atomic positions forming the zig-zag chains along the *a* axis (…-$Tb2^1$ -.$Tb2^4$-$Tb2^1$ -… and …-$Tb2^2$-$Tb2^3$-$Tb2^2$ -…) and on the other, the antiferromagnetic coupling is observed between these zig-zag chains (Fig. 7). This most probably is the origin of the absence of magnetic moment on the Tb1 site.

The temperatures of magnetic transitions of Tb_3NiSi_3 and Dy_3NiSi_3 correspond to de Gennes rule [17], which indicate their same magnetic ordering and the magnetic ordering of Gd_3NiSi_3 should be differs from the ordering of Tb_3NiSi_3 and Dy_3NiSi_3 from de Gennes rule [17].

Thus from this study, below the antiferromagnetic ordering temperature (T_N=202 K and T_N=140 K for Tb_3NiSi_3 and Dy_3NiSi_3, respectively), the Tb_3NiSi_3 and Dy_3NiSi_3 compounds show the antiferromagnetic ordering of *R*2 4*j* sublattice (the $(\mathbf{AF}_a+\mathbf{AF}_c)^{\mathbf{K0}}$ **I′2/m** high-temperature antiferromagnet as for Tb_3NiSi_3). This antiferromagnetic transition corresponds to the relatively low isothermal magnetic entropy change (ΔS_m=−1.2 J/kg K and ΔS_m=−0.4 J/kg K at 146 K in field of 50 kOe and 20 kOe, respectively for Dy_3NiSi_3). Below the spin-reorientation temperature (T_{SR}=132 K and T_{SR}=99 K for Tb_3NiSi_3 and Dy_3NiSi_3, respectively), the Tb_3NiSi_3 and Dy_3NiSi_3 show the spin-reorientation behavior of *R*2 4*j* sublattice (the $(\mathbf{AF}_a+\mathbf{AF}_b+\mathbf{AF}_c)^{\mathbf{K0}}$ **I′i** low-temperature antiferromagnet as for Tb_3NiSi_3). This spin-reorientation transition also corresponds to a relatively low isothermal magnetic entropy change, (ΔS_m=−1.1 J/kg K and ΔS_m=−0.4 J/kg K at 92 K in field of 50 kOe and 20 kOe, respectively for Dy_3NiSi_3). We suggest the metamagnetic-like ordering (or transformation of pure antiferromagnet into a material with mixed ferromagnetic–antiferromagnetic interactions or noncollinear ferromagnetism) of the *R*2 4*j* sublattice in Tb_3NiSi_3 and Dy_3NiSi_3, only because even in field 140 kOe the resulting saturation magnetization corresponds to the ferromagnetic ordering the *R*2 4*j* sublattice, only (22 μ_B/fu for Dy_3NiSi_3 at 2 K).

6. Conclusions

This work establishes complex field sensitive antiferromagnetic

Table 5
Crystallographic and magnetic parameters of the Y_3NiSi_3-type Tb_3NiSi_3 compound as refined at different temperatures: unit cell data, $\mathbf{M}_{a\mathrm{Tb2j}}^{\mathbf{K0}}$, $\mathbf{M}_{b\mathrm{Tb2j}}^{\mathbf{K0}}$ and $\mathbf{M}_{c\mathrm{Tb2j}}^{\mathbf{K0}}$ the magnetic moments of $Tb2^j$ atom along the *a*, *b* and *c* axis of unit cell, respectively and $|\mathbf{M}_{\mathrm{Tb2}}^{\mathbf{K0}}|$ the resulting magnitude of Tb2 magnetic moment ($\mathbf{K}_0=[0, 0, 0]$ propagation vector). R_F (crystal structure) and R_F^m (magnetic structure) are reliability factors.

T (K)	Unit cell data	R_F (%)	Atom	$M_{a\mathrm{Tb2j}}^{K0}$ (μ_B)	$M_{b\mathrm{Tb2j}}^{K0}$ (μ_B)	$M_{c\mathrm{Tb2j}}^{K0}$ (μ_B)	$\lvert M_{\mathrm{Tb2}}^{K0}\rvert$($\mu_B$)	R_F^m (%)
Paramagnet								
298[a]	$a=0.39567(2)$ nm	2.4						
	$b=0.41217(2)$ nm							
	$c=1.74059(9)$ nm							
250	$a=0.39654(9)$ nm	5.8						
	$b=0.41339(9)$ nm							
	$c=1.7456(4)$ nm							
HT **Antiferromagnet at 180 K, 170 K and 150 K.**								
***a*-Antiferromagnet** and ***c*-Antiferromagnet of I′2/m magnetic space group:** $(\mathbf{AF}_a+\mathbf{AF}_c)^{\mathbf{K0}}$**I′2/m**								
150	$a=0.39591(8)$ nm	4.7	$Tb1^1$	0	0	0	0	4.4
	$b=0.41195(7)$ nm		$Tb1^2$	0	0	0		
	$c=1.7436(4)$ nm		$Tb2^1$	+5.29(5)	0	+2.5(1)	5.84(7)	
			$Tb2^2$	−5.29(5)	0	−2.5(1)		
			$Tb2^3$	−5.29(5)	0	−2.5(1)		
			$Tb2^4$	+5.29(5)	0	+2.5(1)		
LT **Antiferromagnet at 125 K down to 1.5 K.**								
***a*-Antiferromagnet,*c*-Antiferromagnet** and ***c*-*Anti*ferromagnet of I′i magnetic space group:** $(\mathbf{AF}_a+\mathbf{AF}_c+\mathbf{AF}_c)^{\mathbf{K0}}$**I′i**								
75	$a=0.39571(8)$ nm	4.4	$Tb1^1$	0	0	0	0	4.3
	$b=0.41175(7)$ nm		$Tb1^2$	0	0	0		
	$c=1.7434(4)$ nm		$Tb2^1$	+5.5(1)	+4.0(2)	+3.3(2)	7.6(1)	
			$Tb2^2$	−5.5(1)	−4.0(2)	−3.3(2)		
			$Tb2^3$	−5.5(1)	−4.0(2)	−3.3(2)		
			$Tb2^4$	+5.5(1)	+4.0(2)	+3.3(2)		
1.5	$a=0.39566(8)$ nm		$Tb1^1$	0	0	0	0	3.3
	$b=0.41166(7)$ nm		$Tb1^2$	0	0	0		
	$c=1.7439(5)$ nm		$Tb2^1$	+5.9(1)	+4.3(2)	+3.7(2)	8.2(1)	
			$Tb2^2$	−5.9(1)	−4.3(2)	−3.7(2)		
			$Tb2^3$	−5.9(1)	−4.3(2)	−3.7(2)		
			$Tb2^4$	+5.9(1)	+4.3(2)	+3.7(2)		

[a] X-ray powder data.

nature of Y_3NiSi_3-type {Gd, Tb, Dy}$_3NiSi_3$ compounds. The partial magnetic ordering of rare earth sublattice (*R*2 4*j* sublattice, only) in R_3NiSi_3 is an interesting observation in the family of magnetically ordered rare earth intermetallic compounds.

Acknowledgments

The Institute Laue Langevin (Grenoble, France) is warmly acknowledged for the use of the neutron diffraction beam. SKM thanks CAPES, Brazil for the award of a fellowship during the course of this work. This work was supported by the Indo-Russian Fund for Basic Research through the project N° 15-53-45129-a.

References

[1] F. Merlo, M.L. Fornasini, M. Pani, J. Alloy. Compd. 387 (2005) 165–171.
[2] Pearson's Handbook of Crystallographic Data for Intermetallic Phases, American Society for Metals, Metals Park, Oh 44073 1-3 (1985).
[3] SpringerMaterials The Landolt-Börnstein Database-Materials Science Data for 250000 Substances. Available at: ⟨http://www.springermaterials.com⟩.
[4] Available at: ⟨www.ill.eu⟩, Yellow Book.
[5] F. Izumi, in: R.A. Young (Ed.), The Rietveld Method, 13, Oxford University Press, Oxford, 1993.
[6] F. Izumi, Rigaku J. 6 (1) (1989) 10–20.
[7] R.A. Levy, Principles of Solid State Physics, Academic Press, 1968.
[8] A.M. Tishin, Y.L. Spichkin, The Magnetocaloric Effect and Its Applications, Institute of Physics Publishing, Bristol, Philadelphia (2003), p. 480.
[9] J. Rodriguez-Carvajal, Physica B 192 (1993) 55–69.
[10] C.J. Bradley, A.P. Cracknell, The Mathematical Theory of Symmetry in Solids, Clarendon, Oxford, 1972.
[11] O.V. Kovalev, Representations of the crystallographic space groups, second ed., Gordon and Breach Science Publishers, 1993.
[12] Fizicheskie velichiny (Physical Data). Handbook. Ed. by I.S. Grigor'ev, E.Z. Meilohov, Moscow, Energoatomizdat, 1994 (*In Russian*).
[13] J. Emsley, in: The elements. Second edition, Clarendon press – Oxford (1991).
[14] L.D. Tung, K.H.J. Buschow, J.J.M. Franse, N.P. Thuy, J. Magn. Magn. Mater. 154 (1996) 96.
[15] V.N. Nguyen, J. Rossat-Mignod, F. Tchéou, Solid State Commun. 17 (1975) 101–105.
[16] J. Pierre, a S. Auffret, B. Lambert-Andron, R. Madar, A.P. Murani, J. L. Soubeyroux, J. Magn. Magn. Mater. 104–107 (1992) 1207–1208.
[17] S. Legvold, in Rare Earth Metals and Alloys, Ferromagnetic Materials (E.P. Wohlfarth, Edit.), Amsterdam, North-Holland Publish. Comp. (1980), pp. 183–295.